Journal Pre-proofs

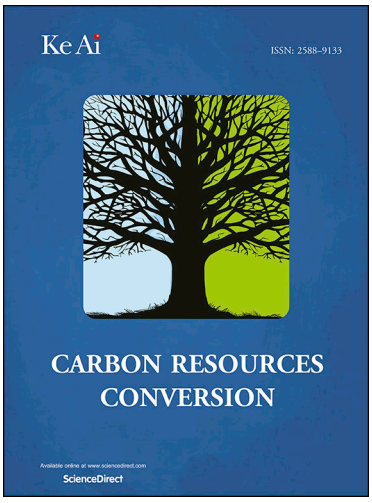

Original Article

One step preparation of papyrus culm derived activated biochar using partial air oxidation and its use as a filter for water treatment in aquaponics culture

Sumrit Mopoung, Suthasinee Pantho

PII: S2588-9133(25)00003-1
DOI: https://doi.org/10.1016/j.crcon.2025.100305
Reference: CRCON 100305

To appear in: *Carbon Resources Conversion*

Received Date: 7 October 2024
Revised Date: 13 January 2025
Accepted Date: 25 January 2025

Please cite this article as: S. Mopoung, S. Pantho, One step preparation of papyrus culm derived activated biochar using partial air oxidation and its use as a filter for water treatment in aquaponics culture, *Carbon Resources Conversion* (2025), doi: https://doi.org/10.1016/j.crcon.2025.100305

One step preparation of papyrus culm derived activated biochar using partial air oxidation and its use as a filter for water treatment in aquaponics culture

Sumrit Mopoung* and Suthasinee Pantho

Chemistry Department, Faculty of Science, Naresuan University, Phitsanulok, Thailand, 65000.

* Corresponding author, E-mail: sumritm@nu.ac.th

Abstract

Papyrus culm derived activated biochars were prepared through carbonization and air oxidation at 400-600°C. The activated biochars were analyzed by SEM-EDS, FT-IR, Raman, BET, and XRD techniques. The best product was collected for use as filter material in aquaponics. It was found that the activated biochars have diverse properties with high disorder of graphitic, oxygenated functional groups (OH, C=O, C-O, and Si-O), oxide compounds (CaO, MgO, Na_2O, K_2O, SiO_2), and relatively high specific surface area and micropore volume. These parameters increased with increasing carbonization temperature from 400°C to 600°C. For materials produced at 600°C the pore size of the derived activated biochar falls in the range of micropores (< 2 nm), with a small mesopore and macropore content. This product has BET specific surface area of 270.27 m^2/g. Utilizing the derived activated biochar prepared with carbonization at 600°C for aquaponics culture has shown that the values of total NH_3, NO_2^-, NO_3^-, PO_4^{3-}, and turbidity decreased, while the DO content increased in the water of the aquaponics culture with efficiency percentage values of 33.33-35.90%, 4.93-13.43%, 9.15-12.90%, 34.97-43.04%, 10.23-23.90%, and 16.86-23.90%, respectively, throughout the four weeks of the experiment. This was achieved via electrostatic attraction, exchangeable cation and anion attraction, and filtration. Furthermore, the activated biochar could also maintain the water pH in a relatively alkaline range for the duration of the experiment, which is suitable for cultivating tilapia and growing red oak lettuce. However, the activated biochar filter began to reach sorption saturation during the third week of the experiment. Therefore, the activated biochar filter should be replaced with a new one after four weeks of use. This research has shown that activated biochar from papyrus culm can be a candidate for an adsorbent material with a simple, cost-effective, and timesaving production.

Graphical Abstract

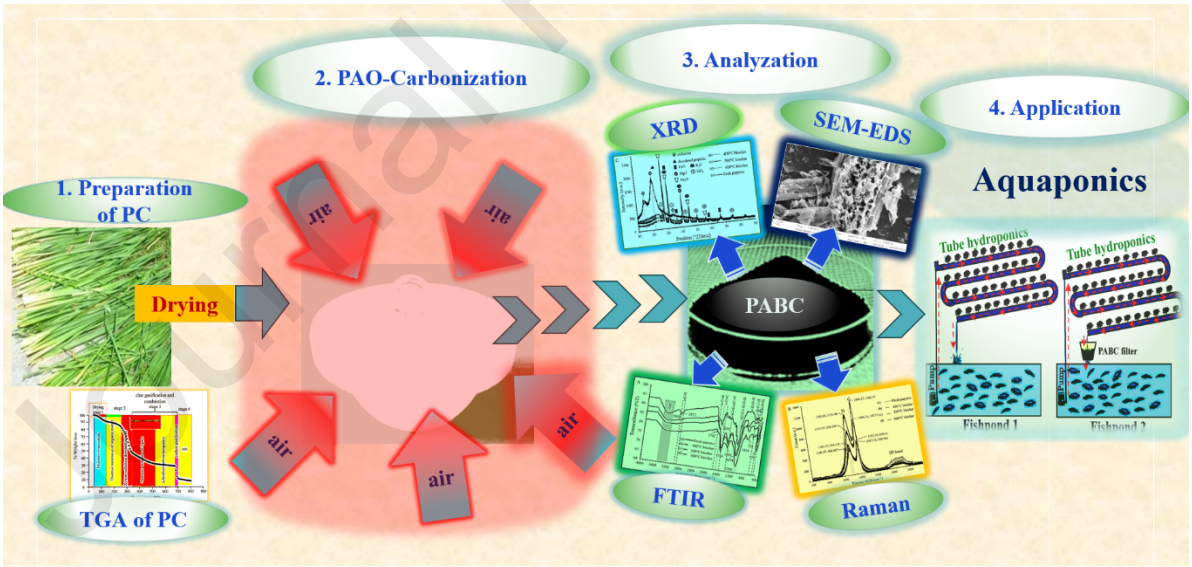

Highlights

• Papyrus culm derived activated biochar production by single step air activation could reduce the cost and production time.

• The best properties of the activated biochar were achieved with activation at 600°C.

• Derived activated biochar could maintain water for culture of tilapia and red oak lettuce.

Keywords Activated biochar; Partial air oxidation; Adsorption; Water treatment; Aquaponics

1. Introduction

A current trend of eco-friendly, cost-effective, and facile methods of production can be observed for carbon-based materials (production from biomass) [1]. Biomass can be converted into biochar (BC), bio-oil, and syngas by thermochemical processes in a limited oxygen environment [2]. Biochar-based materials, which can take the form of hydrochar, pyrochar, engineered biochar, activated biochar (ABC), and biochar-based composites, have been extensively developed by thermochemical processes for various advanced applications [3]. There have been many reports on the applications of BC in various fields such as CO_2 capture, energy storage [4], soil amendments for resource recovery, water retention and plant performance [2], catalytic conversion [3], and removal of pollutants from soil and aqueous environment [5], with agronomic and economic benefits [4]. It can also be used in the development of hybrid techniques for water purification, such as BC-augmented biofilters, permeable reactive barriers, and BC-based membrane filtration [6]. In addition, lignin-sulfonate sulfur-doped mesoporous carbon materials have been used for sodium diclofenac and reactive orange 16 dye adsorptions, and as electrodes for supercapacitors with high efficiencies [7]. Nitrogen-doped activated biochar, which was preparated from spent mushroom substrates by H_3PO_4 activation [8], and cellulose fiber doping with H_3PO_4 and KOH activation [9], was used for removal of reactive orange-16 (RO-16) azo dye and acetaminophen and amoxicillin from water, respectively. The types of thermochemical processes commonly used are hydrothermal carbonization, gasification, flash carbonization, and torrefaction [4]. These processes result in high specific surface area, porosity, and capacity to absorb a wide range of contaminants with high stability of the BC derived from biomass [4]. In addition, BC, which has heterogeneous composition (oxides minerals and oxygen-containing functional groups), can also provide rich and varied surface chemistry, exhibiting various basic, acidic, hydrophobic, and hydrophilic groups [6]. However, the development of these characterstics requires high temperatures in the range of 800-1000°C [6]. When prepared in low temperature conditions, BC suffers from low porosity and/or poor surface functionality, which limits its performance [3]. Therefore, it is necessary to reduce the temperature by the modification or activation of BC products to enhance the beneficial sorption characteristics. In general, activation methods consist of physical techniques (by gas, steam, and mechanical activation), chemical techniques (in the presence of chemicals and inert gas), and biological techniques (microorganisms possessing different metabolic pathways) [6]. In terms of physical techniques, oxygen-containing groups on BC surface could be developted under atmospheric O_2 and/or other gases (e.g., CO_2, NO, and O_3) or solutions with economical reagents and no residual impurities [6]. Atmospheric air, which consists of 20.946 vol. % oxygen [10], is a potential source of oxygen for oxidation during the carbonization process. Air oxidation is one of physical techniques used for the improvement of BCs by development of both pores and oxygenated functional groups on the surface of biochars. Furthermore, it is a simple and favorable green process without the need for

extra chemicals. It is also energy saving due to the exothermic nature of carbon–oxygen reaction [3]. Recently, air oxidation has been extensively applied as a pre-oxidation, post-oxidation, and combined pre- and post-oxidation modification without inert atmosphere for ABC production. This approach provides heat through the exothermic biochar-oxygen and/or volatile-oxygen reactions, initiating the primary thermal degradation of biomass and the subsequent secondary reactions [3], [6]. However, the exothermic nature of air oxidation makes the reaction difcult to control in comparison to CO_2 and H_2O. Futhermore, air oxidation activavation requires the use of specifc temperature for a certain time, where higher O_2 concentration facilitates pore development [3]. Several sources of biomass can be used for BC production such as woody biomass, agricultural waste, municipal solid waste, and sewage sludge [4]. BCs have also been produced from wheat straw, rye straw, wood residues, cherry stone, sewage sludge, and cattle manure under H_2O_2 physical oxidation [11]. Cyperus papyrus (family *Cyperaceae*) is a plant biomass with high production rate (6.00 kg/m^2/year) [12], [13]. It has been planted in a wastewater treatment system for reuse in agriculture by removing heavy metals and antibiotics from wastewater [14]. It was used for biochar preparation under a N_2 atmosphere [15], and activated carbon preparation by sulfuric acid and phosphoric acid activation [16]. However, it has not been used in the preparation of biochar under air oxidation. Therefore, in this research the papyrus plant was selected as a substrate for BC production to be used as a filter in an aquaponics system (AS). It is well known that AS is a combination of aquaculture and vegetable hydroponics culture used for solving population growth, urbanisation, water shortages, land and soil degradation, environmental pollution, world hunger, and climate change [17]. This system enables sustainable, efficient, and intensive food production with high quality production yield, which allows the fish, plants, and bacteria to thrive symbiotically and to work together to create a healthy and balanced growing environment for each other [18]. However, the water in this system still has problems with nitrogen componnds (e.g. ammonia, nitrite, nitrate), phosphate, and turbidity, which affect the pH value and dissolved oxygen (DO). This in turn effects the ecological balance and the growth efficiency of the plants and animals. Current ASs use different species of fish. One of the most common species in ASs is tilapia. This is because of its omnivorous nature, rapid reproduction, and rapid growth [19]. Finally, the type of plant also effects the productivity of an AS culture. Usually, herbaceous spcecies of plants (e.g. basil, peppermint, spearmint, coriander, chives, parsley, tomato, pak choi, lettuce, spinach, chard, Chinese cabbage, watercress, calendula, zinnia, and cucumbers), which require high nutrient consumsion, are popularly grown in ASs [19], [20], [21].

This research studied the ABC preparation from papyrus culm (PC) using one step partial air oxidation (PAO) without the use of an inert gas along with carbonization in the temperature range between 400°C and 600°C for use as filter in AS. The objective of the research was to find suitable carbonization temperature using atmospheric air for simple, easy, low cost, time and energy saving, and green process. The thermal behavior of the dried raw PC was analyzed by differential scanning calorimetry and proximate analysis. FTIR, Raman spectroscopy, XRD, SEM-EDS, BET and proximate analysis were used for the analysis of the dried raw PC and ABC products. Finally, the collected ABC with the best characteristics was used as filter for water treatment in an AS.

2. Materials and methods

2.1. Preparation of raw PC and ABC

2.1.1. Preparation of raw PC

The PC was obtained from Phitsanulok province, Thailand. It was sun dried for 2 weeks and cut into pieces 2-3 cm long. The thermal behavior of the dried raw PC was investigated as a function of pyrolysis temperature in N_2 atmosphere with differential scanning calorimetry (DSC-1, Mettler, Columbus, USA) between 30°C and 800°C. The dried raw PC was analyzed for proximate composition, including moisture [22], ash [23], volatile mater [24], and fixed carbon [25].

2.1.2. Preparation of ABC

Samples (20 g, OHAUS; Scout Pro, USA) of dried raw PCs were loaded into a crucible with a lid and placed in an electric furnace (Fisher Scientific Isotemp® Muffle Furnace, *Pennsylvania,* USA) for PAO without inert gas along with carbonization at 400°C, 500°C, or 600°C for 0.5 h. After that, the samples were cooled to room temperature. The final products are papyrus culm derived activated biochar (PABC) products. The percent yields of the PABC products were calculated. The PABC products were kept in a desiccator for further analysis and experiments.

2.2. Characterization of PABCs

The PABC products were characterized by FTIR (Spectrum GX, Perkin Elmer, Connecticut, USA) to classify the organic and inorganic chemical bonds or functional groups. Raman spectroscopy (Bruker, MultiRAM, Vienna, Austria) was used to find the carbon crystallinity of products. XRD (PW 3040/60, X' Pert Pro Console, Philips, Netherland) was used to analyze and identify the type of compounds and crystal structure. SEM-EDS (Leo1455VP Electron Microscopy, Cambridge, England) was used to study the surface characteristics, size, shape, and the elemental composition. BET (Micromeritics TriStar II3020, Bavaria, Germany) was used to analyze the specific surface area, pore volume, average pore size, and pore size distribution of the PABC products. Proximate analysis was also used to determine the proximate composition of the PABC products. Finally, the collected PABC with the best characteristics was used for water treatment in aquaponics culture.

2.3. Construction of AS

Two fishponds, width 2 m. x length 2 m. x height 70 cm., were built with interlocking bricks and lined with 2 layers of plastic sheets. After that, 2 m^3 volume of water was added to each pond achieving a depth of 50 cm. The fishponds were covered with netting to prevent anything falling into the ponds. Meanwhile, two tubular hydroponic systems with width 2 m, length 4 m, 2 % slope, and height of approximately 30 cm from the fishponds, were built with 4 m of 5 cm diameter PVC pipe. Holes with a diameter of 4.1 cm and a separation of 20 cm were drilled into the pipes. Six interconnected pipes were used and fixed with steel angles on each panel. The tubular hydroponics system has a tube length of 24 meters with 120 holes. Two ASs were used for the experiments.

Aquaponics system 1 was operated without a PABC filter tank (Fig. 1a). PABC filter tank, which contained 3 kg of PABC, was placed between fishpond 2 and hydroponics panel 2 (Fig. 1b). Water from both fishponds was circulated through hydroponics tubes by electrical pumps with a 120 L/h flow rate. The schematic for the ASs experiments is shown in Fig. 2.

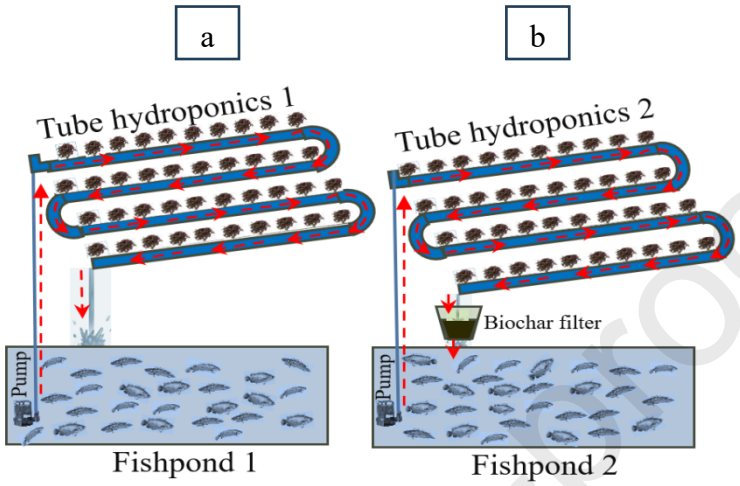

Fig. 1. ASs (a) without biochar filter, and (b) with biochar filter

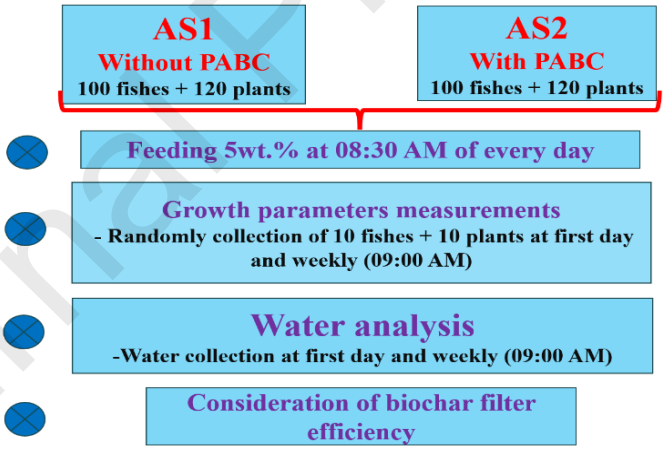

Fig. 2. Schematic for the aquaponics system experiments.

2.3.1. Aquatics system experiment

The aquatic system in both ponds was filled with one hundred small Nile tilapia [*Oreochromis niloticus* (Linn.)] fish with body length of approximately 2-3 cm. Fish food, 5% of the weight of the average fish weight in each pond, was fed into the ponds every day at 08:30 AM. Ten fish were randomly collected and weighed at the beginning of the experiment and once every week for growth rate calculation.

2.3.2. Hydroponics system experiment

Sponges with the size of 2.5 cm x 2.5 cm x 2.5 cm, which were soaked with water, were used to grow red oak lettuce seeds for 7 days. After that, the sponges were transferred into the holes in the hydroponic tube system for planting. Ten red oak lettuce plants were randomly collected for growth rate measurement with parameters of stem height, root length, number of leaves, and canopy diameter on the first day of the culture and weekly throughout the experiment. In addition, fresh stem weight, dried stem weight, fresh root weight, dried root weight, fresh leaves weight, and dried leaves weight were analyzed after 4 weeks of culture.

2.3.3. Water analysis

Water samples were collected from each pond within 20 cm water depth into plastic bottles with a lid at first day of the culture and weekly throughout the experiment at about 09:00 AM. Parameters of turbidity, pH, total ammonia, nitrite, nitrate, orthophosphate, and DO were measured. Turbidity and pH of water were measured by turbidimeter (Jenway 6035, Chelmsford, England) and pH meter (Mettler Toledo, Hamilton, New Zealand), respectively. For the measurements of total ammonia, NO_2^-, NO_3^-, PO_4^{3-}, and DO, the water samples were filtered through a Whatman No.42 filter paper. Total ammonium, nitrite, and nitrate were determined by indophenol reaction [26], the diazotization colorimetric method [27], spectrophotometric method [28], and orthophosphate method using ascorbic acid [29], respectively. The resulting solutions were measured by UV-Vis spectrophotometer (double beam, Jasco V650, Maryland, USA) at 655 nm, 507 nm, 220 nm, and 880 nm for concentration measurements of total ammonia, NO_2^-, NO_3^-, and PO_4^{3-}, respectively. DO was also measured by titration with sodium thiosulphate [30]. The percent relative removal rate was used for evaluating the removal efficiency of total ammonia, NO_2^-, NO_3^-, PO_4^{3-}, and turbidity from water and increasing content of DO in water by biochar filter.

$$\text{Relative removal (or augmentation) rate (\%)} = [(C_0-C_t)/C_0] \times 100\ \% \quad (1)$$

Where C_0 refers to the concentration of the experiment control system (Fishpond 1), and C_t refers to the concentration of experiment system 2 (Fishpond 2) for consideration of biochar filter efficiency.

3. Results and discussion

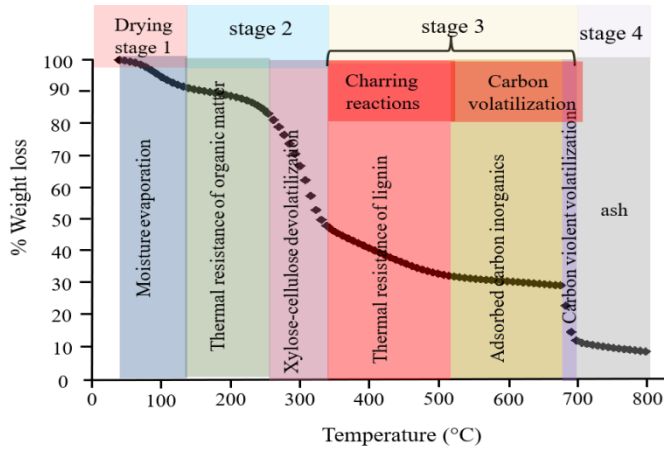

Fig. 3 TGA curve of dried raw PC.

Table 1. Percent yield and proximate composition of dried raw PC and PABCs.

Samples	Temperature °C	% yield	Moisture wt.%	Volatile matter wt.%	Ash wt.%	Fixed carbon wt.%
dried PC			5.58±0.58	61.70±0.75	7.69±0.71	25.12±1.94
PABC	400	39.17±1.41	1.92±0.21	4.56±0.60	12.73±0.14	80.79±0.42
	500	31.24±2.32	0.93±0.85	2.45±0.49	13.54±0.62	82.94±0.63
	600	29.36±1.29	0.65±0.73	0.91±0.09	14.61±0.08	83.75±0.23

3.1. Characteristic of raw PC and PABCs

3.1.1. Thermal behavior of raw PC

The TGA curve of dried raw PC acquired under nitrogen atmosphere in the temperature range from 30°C to 800°C is displayed in Fig. 3. It shows that the weight losses of raw PC take place in four stages. The first stage is moisture evaporation (unbound and bonded on the surface of the PC)

and volatilization of some light organic molecules [31] in the PC, which occurred from 30°C to about 130°C. The weight loss in this stage is about 8%. The second stage occurred in the range between 130°C and 340°C and it is due to thermal resistance of organic compounds, which is related to the thermal decomposition of xylose (173-645°C), cellulose (291-395°C), hemicellulose (100–300°C), and some lignin (170-935°C) [31], [32]. The weight loss is about 45% by devolatilization of these organic compounds at the end of the second stage (260-340°C). The third stage (340-700°C) is charring and carbon volatilization. In the initial part of this stage, thermal resistance of lignin had occurred with slow degradation under the inert atmosphere during charring reaction [33]. It is because of the high temperature resistance of lignin, which requires high energy for the breakdown of double bonds in the structure of lignin [32]. The thermal degradation of lignin occurs gradually until the end of this stage [31]. In addition, volatilization of carbon has also occurred between 520°C and 680°C [32]. This is followed by violent volatilization of absorbed carbon by the inorganics at the end of the third stage until only ash remains (about 7-8%) into the fourth stage [34]. In total, the third stage results in about 39% of weight loss. It can be seen that the ash content of the raw PC is quite high. This is attributed to the accumulation of minerals, which were absorbed from the soil or water, by the plants and resulted in the high ash content [35].

3.1.2. Percent yield and proximate composition

PC was used for ABC prepraration with PAO without innert gas flow along with carbonization temperatures of 400-600°C. These conditions allowed a small amout of atmospheric air to flow through the lid as well as the outflow of thermodegraded volitile matter during the carbonization process. In this process, it is expected that partial oxidation by air takes place without overly extensive oxidation reactions. The results have shown that the PABC yields have decreased with increasing carbonization temperature (Table 1). In general, it has been concluded that the yield of PABC produced at 400-600°C mainly depends on the degradation via dehydration, fission reactions, and increased rate of volatilization of anhydro sugars present in the tar [6]. At carbonization temperature of 400°C, the PABC yield was 39.17±1.41%, and then it dropped sharply for the product made at 500°C. However, the relative decrease in the PABC yield from 500°C to 600°C is smaller. The sharp reduction of the PABC yield from 400°C to 500°C was attributed to rapid reduction of volatile matter content during carbonization at the temperature of 500°C [36]. This could be explained by the fact that the main decomposition of cellulose (240–350°C volatized) and hemicellulose (200–260°C volatized) occurrs below 400°C, while the main decomposition of lignin is in the range of 280°C to 550°C [35]. Therefore, some of the volatile matters, especially uncarbonized lignin, have remained in the PABC product (4.56±0.60%) after carbonization at 400°C. Additionally, a small amount of volatile matters (2.45±0.49%) remained in the PABC product after carbonization at 500°C. Furthermore, lignin can also be converted to fixed carbon by the charring reactions, which occurr at 500°C [32]. Consequently, the relative decrease of percent yield of the PABC products was observed after the carbonization temperature increased from 500°C to 600°C. The results of the TGA analysis (Fig. 3) show the thermal degradation of organic compounds under nitrogen atmosphere, while the carbonization process operated under partial air oxidation with reduced oxygen content. The percent yield results confirm that some matter was oxidized under the partial air oxidation to a higher degree than under nitrogen asmosphere at the same temperature. It was observed that the proximate composition

(moisture, volatile matter, and ash) of dried raw PC (Table 1) is consistent with the TGA result (Fig. 3). After carbonization treatment at 400°C to 600°C, volatile matter content was greatly reduced, while fixed carbon content shows an inversed trend. This is because fixed carbon, which is a solid combustible residue, remains after the expulsion of the volatile matter during heating [35]. It was shown that most of the volatile matters were thermally degraded, while some were converted into fixed carbon by a partial oxidation reaction. In the same way, ash content increased with increasing carbonization temperature due to the thermal breakdown of organic components with the release of CO_2 [31]. This results in the relative enrichment of various inorganic components in the ash form [36] in the remaining material. The moisture content of dried raw PC is only 5.58±0.58% after 2 weeks of sun drying with low costs, which is preferable for thermal conversion as the moisture levels are below the permissible limit (<10 %) for such process [31].

3.1.3. Elemental composition from EDS

The carbon content, content of metal elements, and content of Si in the PABCs increased with increasing carbonization temperature from 400°C to 600°C, while oxygen content is reduced (Table 2). The decrease in oxygen content is related to the breaking of weaker bonds of volatile matters within the PABC structure by water elimination, decomposition of hydrocarbons, tar vaporization, and liberation of H_2, CO, and CO_2 leading to the PABC becoming highly carbonaceous because of the carbonization process [31], [35]. The carbon content increased with increasing carbonization temperature because of intense carbonization occurring at high temperatures and because of having a high content of carbon in aromatic compounds [31]. Considering the O/C ratios of the PABC products, their values are relatively low (0.17-0.22), which implies low polarity [31], high degradation stability, and very stable structural arrangement of the aromatic rings [35]. These ratios decreased with increasing carbonization temperature from 400°C to 600°C. This showed that the carbonaceous and aromatic ring characteristics increase with increasing carbonization temperature. This indicates that the PABCs have a less hydrophilic surface when produced at higher carbonization temperatures [31]. Other inorganic elements have also appeared within the texture of the PABCs in the ash form, which is formed by disproportionately volatilizing the carbon of the plant tissue [36] leading to high residue content. Generally, high ash contents are observed in materials made from grain, straw, and grass husks, which are rich in silica [6]. Likewise, papyrus is also highly effective in retaining mineral elements [14]. The contents of these inorganic elements increased with increasing carbonization temperature from 400°C to 600°C, which causes more organic matter to volatilize and leaves behind a higher percentage of inorganic elements [31]. These elements are in the form of oxide compounds (except Ca and K), which have vaporization temperatures higher than 600°C, and include MgO (1107°C) [36], and SiO_2 (1426-1676°C) [37]. While Ca (in form of $CaCO_3$) and K (in the form of K_2CO_3) are thermally decomposed above 750 °C [38] and 900°C [39], respectively. Na content decreased with increasing carbonization temperature, because it is less stable in the form of an oxide, which was reduced by the carbon-hydrogen fuel matrix to metal vapor [40]. However, Na_2O also has a high melting point of 1132°C [41], which can make it stable at high temperatures. In addition, alkaline metals (especially K) can reduce ash melting point leading to slag and agglomeration on PABC [35]. Furthermore, cell walls in biomass could entrap Ca, K, (by intercalating between graphene sheets or forming phenoxides), Si (as opal phytoliths and silica), and Mg (associated

with organic molecules through covalent and ionic bonds), which can cause the release of these elements at higher temperatures during thermal decomposition [6]. Therefore, these elements were retained in the texture of the PABCs under carbonization temperatures in the range between 400°C and 600°C. Based on these observations, the contents of these elements within the texture of the PABC products increase with increasing carbonization temperature due to higher thermal degradation of volatile compounds at higher carbonization temperatures. It was seen that the raw PC has high ash content. The results for the carbonized products show that the ash contents of the PABCs are also quite high and they exhibit alkaline properties [4].

Table 2 Elemental composition from EDS of PABCs with 400°C-600°C carbonization temperature.

Temperature °C	Elements composition (wt.%)							
	C	O	O/C ratios	Ca	Mg	Na	K	Si
400	78.78	17.06	0.22	0.54	0.56	1.09	1.34	0.63
500	80.94	15.29	0.19	0.63	0.65	0.75	1.58	0.93
600	81.48	13.97	0.17	0.75	0.77	0.53	1.83	1.24

3.1.4. Study of surface functional groups by FTIR

FTIR was used to characterize the chemical composition and analyze the bonds between carbon, hydrogen, and oxygen in PABCs. This information can be used to gain insights about the suitability of PABC products for utilization in environmental and energy applications [42]. Results of FTIR measurement for raw PC revealed the presence of surface functional groups of organic materials, moisture, and residual elements [Fig. 4A(a)]. The surface functional groups included -OH, C-H, C=O, C=C, C-O, Si-O-C, and Si-O-Si. The –OH group is represented by the stretching vibration band between 3200 cm^{-1} and 3500 cm^{-1}, which could originate from moisture, acids, and phenolic constituents of polysaccharides of all organic matters [31]. Surface functional C-H groups are represented by asymmetric and symmetric stretching vibrations with peaks of medium and weak intensities at 2938 cm^{-1} and 2872 cm^{-1}, respectively. These peaks correspond to methyl and methylene groups of alkanes in the structures of xylose, cellulose, hemicellulose, and lignin [31], [32]. The peaks also imply the presence of stable ring structures of organic compounds [42].

The C-H groups are also represented by bending vibrations at 1500–1200 cm^{-1} and 900–500 cm^{-1} [32] with peaks of very weak intensity. Furthermore, C=O and C=C surface functional groups are represented by strong peaks at 1742 cm^{-1} and 1632 cm^{-1}, respectively, which correspond to ethers and esters [31], with reactive nature [42], and alkenes that form the backbone of aromatic compounds [31], respectively. The C-O groups are represented by a strong stretching vibration band at 1000-1100 cm^{-1}, which corresponds to the main glucose structure of cellulose and hemicelluloses [31], [32]. Finally, Si-O-C, and Si-O-Si functional groups are represented by bands at 1080 cm^{-1} (overlap with C-O), and 458 cm^{-1}, which correspond to SiO_2 in organic materials [43]. In addition, the band at 458 cm^{-1} also contains a very weak peak of bending mode of SiO_2 network [44]. After the carbonization process carried out at 400-600°C, the intensities of these peaks change in ways that are related to the carbonization temperature [Figs. 4A(b)-(d)]. The bands corresponding to the OH group undergo relative decrease of intensity with increasing carbonization temperature from 400°C to 600°C. These results are due to dehydration and thermal decomposition of cellulose, hemicellulose [31], and lignin [32]. However, it was noticed that the OH group is retained in the PABCs. This result is attributed to the formation of H_2O by degradation of xylose, cellulose, and lignin [32]. It could also be due to the presence of alcohols, phenols, or other hydroxyl-containing compounds [42] formed by the degradation of polysaccharides during the carbonization followed by H-bond reformation with aromatic and graphitic moieties [31], [42] on the surface of the PABC. Likewise, bands for C-H and C=O groups exhibited very low intensity at 400°C and disappeared completely at 500-600°C. This is due to the destruction of methoxy, methyl, methylene, ether, and ester groups of organic compounds leading to the formation of CH_4, CO_2, CO, and H_2O molecules [32]. The C=C bond (peak at 1630 cm^{-1}) in the backbone of organic aromatic compounds is transformed to C=C bonds (peaks at 1564 cm^{-1}) of alkenyl structures within the carbon framework [42] of the PABC products. Therefore, the degradation of C-H and C=O groups increased the aromatization [31] of the PABCs during carbonization at high temperatures (about 500-600 °C). At the same time, content of C=O groups (band with maximum intensity at 1384 cm^{-1}) of ketones, aldehydes, carboxylic acids, and carbonate groups [42], [45] on the surface of the PABCs increased with increasing carbonization temperatures. For C-O group of lactones and quinine in hemicellulose, the intensity decreased with the increase in carbonization temperature from 400 to 600 °C, which indicated more extensive decomposition of hemicelluloses at higher carbonization temperatures [31]. At the same time, new C-O groups formed by partial oxidation with oxygen in air [46], which then resulted in the reformation of carboxyl, carbonyl, carbonate, and ester groups on the carbon framework [32], [45]. In addition, carbonate group is also located at 1500–1200 cm^{-1}, 1000-1100 cm^{-1}, and 892 cm^{-1} [45]. This has confirmed that PAO had occurred during carbonization. Finally, peaks corresponding to Si-O-Si functional groups of SiO_2 network on PABCs tended to increase in intensity with increasing carbonization temperatures, which is due to the decomposition of organic matter. Overall, the FTIR results indicate that the reduction in the content of oxygenated functional groups of organic matters within PC during carbonization at 400-600°C, performed with a closed lid but without inert gas flow, has resulted in good PABCs with the formation of some new oxygenated functional groups. In addition, the retained metal elements within the PABCs can act as exchangeable cations through anion attraction [31]. These characteristics of the PABCs with the diverse chemical bonds imply potential utility in environmental applications [42].

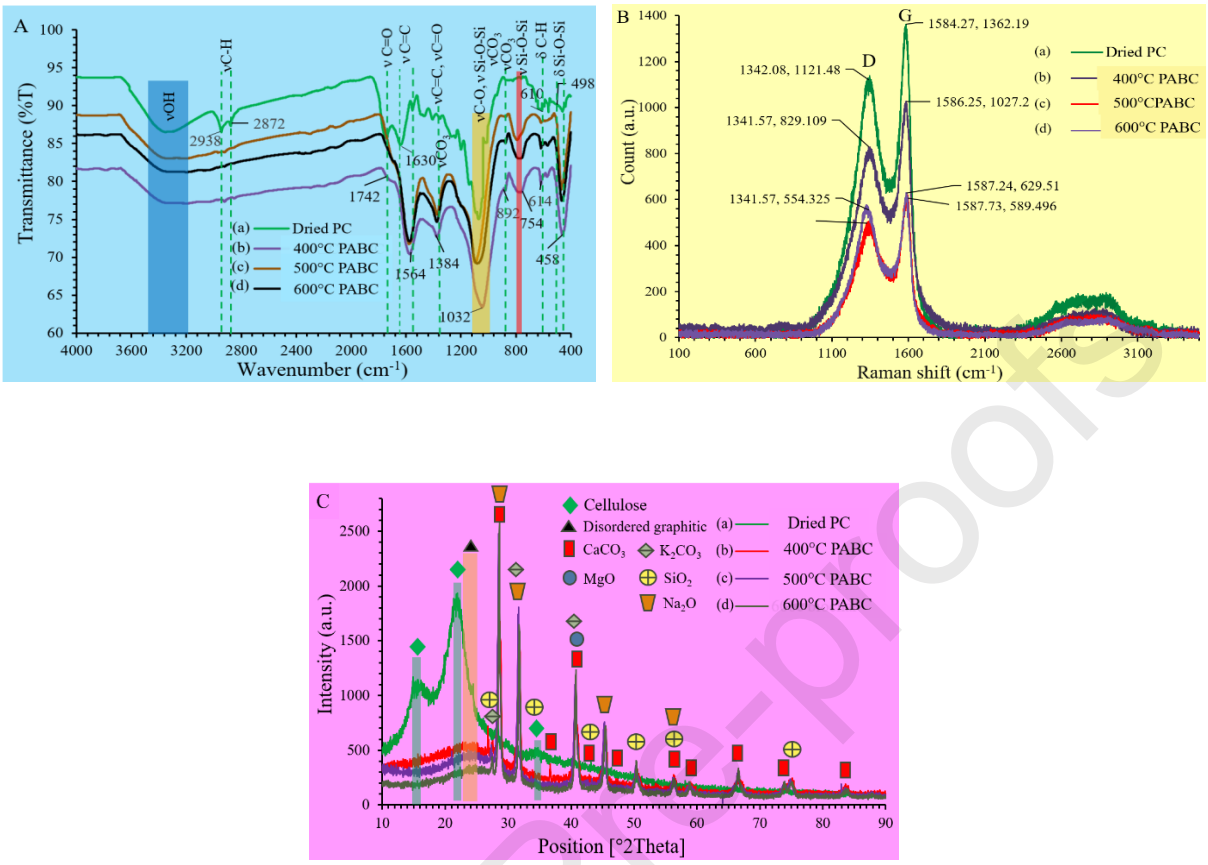

Fig. 4. FTIR transmittance (A), Raman shift (B), and XRD pattern (C), of dried raw PC and PABCs prepared with PAO along with carbonization at temperatures of 400°C-600°C (a)-(d).

3.1.5. Interpretation of Raman shift results

Raman spectroscopy analysis provides information about defects and disorders in addition to the structural information of materials [47]. For carbon based materials, Raman spectra are related to the vibrations of carbon and hydrocarbon structures and usually contain two high intensity peaks D (disorder) and G (graphite) [48]. The Raman spectra of raw PC and PABCs are shown in Figs. 4B(a)-(d). The D peak, which corresponds to lattice defects, disordered arrangement, and low symmetry carbon structures, and G peak, which is the characteristic scattering peak of graphite [47], are located at about 1341 cm^{-1} and 1586 cm^{-1}, respectively. The calculated intensity ratios of D and G peaks of raw PC, and the PABCs preapred at 400°C, 500°C, and 600°C are 0.8233, 0.8072, 0.8150, and 0.8806, respectively. These values indicatate that the PABC product preared by carboniazation at 400°C has a higher degree of graphitization than the raw PC. This result is attributed to crystallite surface of organic functionalization and the content of heteroatoms (O, N, H), which induced the loss of resonant behavior [49] in raw PC, which showed high hydrocarbon characteristics. The contents of these components evolved during carbonization as the organic materials transformed into graphitic structures with highly ordered arrangement. Usually,

amorphous carbon starts transforming into aromatic carbon and polyaromatic graphene sheets at ~330°C and >350°C, respectively [6]. However, while carbon skeleton of organic matters transformed to graphitic structure, carbon lattice defects or disorder in the PABCs were formed by PAO during carbonization, which increased with increasing carbonization temperatures, especially at 600°C. It was shown that graphitic structures were destroyed during carbonizations with PAO at high temperatures. This resulted in a more amorphous carbon structure containing functional groups such as OH, C=O, and C-O, which are usually formed on the surface of PABC by the reduction or carbonization process and are also leveling the disorder degree of the graphitic structure [50]. Another effect is the content of heteroatoms (e.g. Na, Ca, Mg, K, and Si) within the PABCs. These elements, which are distributed irregularly on the surface of the PABCs, can also induce the loss of resonant behavior [49]. Finally, the presence of second-order spectrum 2D band (the second order of the D-band) in the area between 2500 cm^{-1} and 3200 cm^{-1}, which also includes overtones and/or a combinations of the G line and the disorder-induced D component, also indicate high disorder level in graphitic materials [50] in the PABC materials.

3.1.6. XRD patterns

The XRD pattern of the raw PC [Fig. 4C(a)] shows peaks of cellulose, which is composed of glucose monomer units in the form of linear chains and combined into a polycrystalline structure [51], at 2θ values around 15-16.5°, 21.5-22.6°, and 34.5-35° [52]. While hemicellulose (with branched and straight polymer chains) and lignin (three-dimensional polymer) are amorphous. Therefore, these two components do not exhibit peaks in the diffractogram [51]. Diffraction peaks of cellulose are absent, after carbonization at 400-600°C, [Figs. 4C(b)-(d)]. This revealed that all celluloses were decomposed already at the carbonization temperature of 400°C. In addition, most of the remaining non-carbon atoms were removed at carbonization temperatures higher than 600°C [6]. At the same time, the broad bands observed in all PABCs have appeared at 2θ values around 23-25° and 43-44.5°, which correspond to amorphous carbon and graphitic carbon, respectively [53]. This indicated that the characteristic form of the PABCs is a low crystalline carbon structure, which is in aggreement with the results of the Raman spectroscopy (Fig. 4B). In addition, many sharp peaks can be observed in the diffractograms of the PABCs, which correspond to $CaCO_3$ (2θ at 28.60°, 36.71°, 40.81°, 43.28°, 47.15°, 56.33°, 58.88°, 66.62°, 74.03°, and 83.92° [54]), MgO (2θ at 41° [55]), Na_2O (2θ at 28.5°, 31.5°, 45.5°, and 56.5° [56]), K_2CO_3 (2θ at 28.30°, 31.68°, and 40.76° [57]), and SiO_2 (2θ at 26.5°, 34.5°, 43°, 50.5°, 56.5°, and 75.5° [58]). Usually, the metal carbonates were formed by reaction of CO_2 derived components and metal components during carbonization and then thermal decomposed to metal oxides at high temperatures [59]. These metal carbonates decomposed to metal oxides at a temperature not exceeding 600°C [$MgCO_3$ (306-520°C) [59], Na_2CO_3 (337-435°C) [60]], except $CaCO_3$ and K_2CO_3, which decompose at 750 °C [38] and 900°C [39], respectively. These peaks exhibit progressive increases in intensities with increses of carbonization temperature from 400°C to 600°C due to more extensive decomposition of organic matters, which corresponds to the EDS results (Table 2).

3.1.7. Surface morphology of PABCs

SEM images of the PABC products made under atmospheric air with carbonization at 400-600°C are shown in Fig. 5. It can be observed that the PABC, which was produced at 400°C [Fig. 5(a)], reveals open pores with fractures, disorder, and honeycomb-like structure made by transformation from an aromatic structure [31]. Appearance of these pores is attributed to thermal degradation of organic matter [35] within the surface cells of PC during the carbonization process. These characteristic features were formed from the carbon and mineral skeletal structure and porosity of the original biomass [6]. Similar structures can also be found in the PABC prepared with carbonization at 500°C [Fig. 5(b)]. However, it was seen that the surface cells of PC are more extensively decomposed in the 500°C-PABC, including more falling off, and the core begining to emerge more clearly on the surface in comparison to the 400°C-PABC. However, a clear and regular pattern with some fractured pores is formed after carbonization at 600°C [Fig. 5(c)]. Furthermore, tubular structures with macro sized cores have clearly appeared within the 600°C-PABC. These tubular structures were transformed from xylem and phloem of the plant stem [31]. Porosity with tubular structures plays a crucial role in both enlarging the specific surface area

and potentially enhancing the absorption/adsorption capacity [42] of PABC.

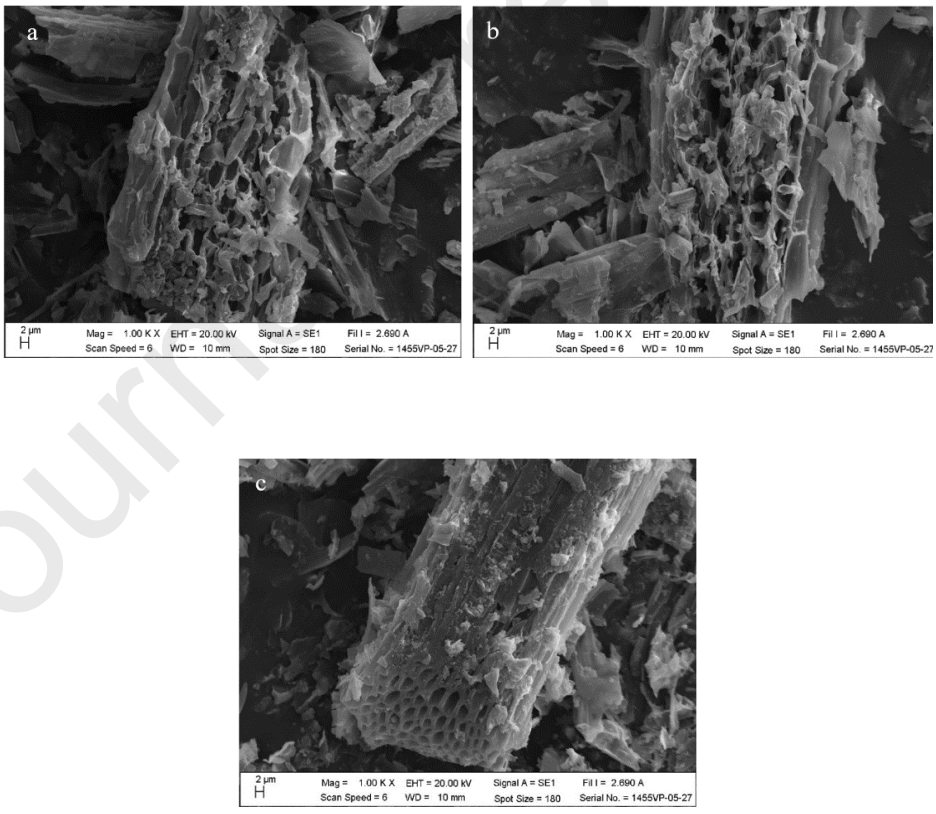

Fig. 5. SEM morphologies of PABCs prepared with PAO along with carbonization at temperature of (a) 400°C, (b) 500°C, and (c) 600°C.

Table 3 Textural characteristics of PABCs by PAO along with 400-600°C carbonization temperatures.

PABCs at carbonization temperature (°C)	BET Surface area (m^2/g)	Micropore volume (cm^3/g)	Total pore volume (cm^3/g)	Average pore size (nm)
400	4.49	0.000361	0.008689	32.5202
500	4.86	0.000752	0.009027	23.8534
600	270.26	0.065577	0.114768	2.14755

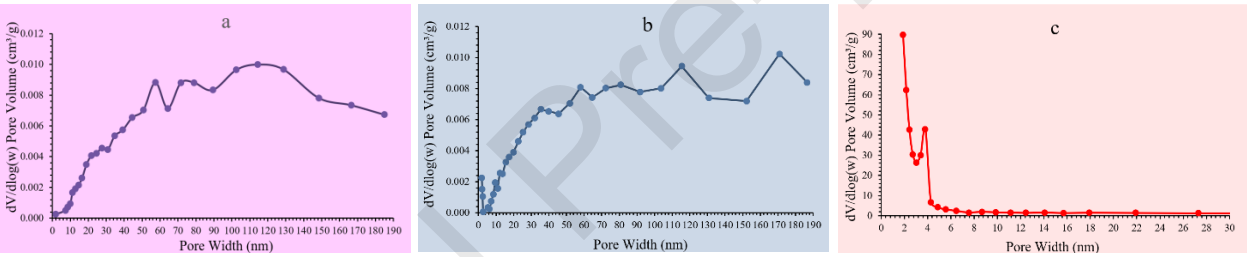

Fig. 6. Pore size distribution of PABCs prepared with PAO along with carbonization at temperature of (a) 400°C, (b) 500°C, and (c) 600°C.

3.1.8. Specific surface area and porosity of PABCs

The porous structure of the PABCs has appeared after PAO along with carbonization, which was attributed to the removal of volatile content during carbonization [35], and partial oxidation of surface carbon [46]. The formation of the porous structure could increase the overall specific surface area [61] of the PABCs. The textural characteristics of the PABCs are shown in Table 3. The results of the BET specific surface area analysis of the PABCs indicates that the specific surface areas increased with increasing carbonization temperatures from 400°C to 600 °C. However, increasing the carbonization temperature from 400°C to 500°C resulted only in a small increase in the BET specific surface area. It was expected, based on SEM morphologies [Figs. 5(a)-(b)], that mainly organic compounds were thermally decomposed on the surface cells of PC. However, the increase of specific surface area in the temperature range 400-500°C was attributed to the formation of free radicals by low atmospheric O_2 levels during the initial carbonization stages, which transformed into carboxyl and carbonyl groups on the surface of the PABCs. These

surface functional groups covered the surface of the PABCs resuling in limited specific surface area increase [6]. On the other hand, increasing the temperature from 500°C to 600°C led to a sharp increase in the BET specific surface areas, which was attributed to a more extensive partial oxidation of surface carbon on the PABCs during 500°C to 600°C carbonization leading to clear formation of open pore structures [Fig. 5(b)]. Other parameters such as micropore volume and total pore volume also increased in line with the BET specific surface areas. Average pore size decreased with increasing carbonization temperature from 400°C to 600 °C, but the main sharp decrease takes place upon increasing the carbonization temperature from 500°C to 600°C. This is attributed to the convertion of macropores in raw biomass into meso and micropores by PAO during carbonization [6]. Considering the pore size distribution of the PABCs (Fig. 6), it can be seen that most pore sizes fall in the range of mesopores (2-50 nm) and macropores (>50 nm) for PABCs made with carbonization at 400°C and 500°C [Figs. 6(a)-(b)]. On the other hand, pore sizes of the PABC made by carbonization at 600°C fall in the range of micropores (< 2 nm) with a small content of mesopores and macropores [Fig. 6(c)]. These results led to the decrease of the average pore sizes of the PABCs with rising carbonization temperature from 400°C to 600°C. Furthermore, open and clearly porous PABC formed at 600°C indicating the opportunity for PAO due to the presence of the micropores on the PABC. Therefore, mainly micropores with 2.14755 nm average pore size were developed on the PABC at 600°C, which resulted in specific surface area increasing significantly. It can be seen that the carbonization temperatures during PAO significantly affect the porosity of the PABCs. However, it was found that the BET specific surface areas of the PABCs are quite low, especially for materials made at 400-500°C. This is attributed to high ash content, tars, and some surface fucntional groups, which have accumulated and blocked the pores on the PABC surface. Therefore, low content of open pores was observed on the surface of the PABCs made with carbonization at 400-500°C [35]. Thus, the specific surface area of these products is low.

3.2. Results of aquaponics experiments

3.2.1. Water treatment in AS

Organic materials from fish waste in the water decompose into inorganic matter by the action of various microorganisms, including the nitrification process [62]. Inorganic products consist of phosphates and nitrogenous compounds, which cause physiological changes, morphological changes, and aquatic losses [63]. Organic nitrogen materials are converted to ammonia by microbial action [64]. Subsequently, ammonia is oxidized into nitrite, and then nitrite is oxidized into nitrate by the nitrification process with autotrophic nitrifying bacteria [65]. This process is inhibited at pH values below 5.8 [66]. Nitrite ion, which is produced by the nitrification process, causes brown blood disease (methemoglobin) in fish [63]. Nitrate is a stable and dynamic anion in oxygenated water [64]. However, these inorganic products are uptaken by plants in hydroponic circulation systems [67]. Using adsorbents as filter materials in AS could reduce the content of these inorganic materials. In this study, the PABC made with PAO along with carbonization at 600°C, which has diverse properties including numerous functional groups, many metal elements, high specific surface area, and high micropore volume, was used as a filter for the immobilization of pollutants from solution in AS. Water properties, fish growth, and plant growth were measured

for the evaluation of the effects of the PABC material. The results of the water analysis have shown that total NH_3, NO_2^-, NO_3^-, PO_4^{3-}, and turbidity concentrations in the water of the control aquaponics fishpond 1 were much higher than in the water of the AS fishpond 2 (Figs. 7B-E and 7G). While the order vas inversed for pH and DO values (Figs. 7A and 7F) for all four weeks. This indicated that the PABC filter could improve water quality in AS. The water in fishpond 1 was weakly acidic [Fig. 7A(a)], while the water in fishpond 2 has weakly alkaline [Fig. 7A(b)]. The cause of the acidity of water in fishpond 1 is the higher total ammonia content [68]. Furthermore, the CO_2 from fish breathing can be dissolved in water leading to the formation of HCO_3^- and H^+ resulting in the acidification of the culture water [69]. The pH values in fishpond 2 are related to low ammonium ion concentration, which was adsorbed by the PABC by attractive electrostatic force between the positively charged ammonium ion and negatively charged surface functional groups of PABC resulting in low ammonia content and slightly alkaline water. Furthermore, some alkaline metal oxides from the PABC filter could be released to the water, which can increase pH in fishpond 2 [4]. It was observed that the pH values of water in both fishponds are higher than 5.8, which cannot lead to the inhibition of the nitrification process. Likewise, the phosphate was also adsorbed by PABC in weakly alkaline condition via chelation and complexation with electron donor oxygen containing surface groups on the PABC surface [70]. Alternatively, phosphate ion can also combine with negative oxygen ion and create phosphate esters on the surface of the PABC in alkaline water [70]. Therefore, both ammonia and phosphate ion, which remained after absorption by plant roots in the hydroponics systems, were adsorbed by the PABC filter in aquaponics system 2 (AS2). In the case of nitrite [Figs. 7C(a) and (b)], which is slightly less harmful to fish than ammonia, but makes it more difficult for fish to take up oxygen [71], its concentrations were initially high in both systems due to low microbial conversion of ammonia to nitrite during the initial stages of nitrification. However, nitrite concentration decreased and became relatively stable in the range between 0.0122 mg/L and 0.0210 mg/L after one week. This is lower than the limit of methemoglobin (1.38 mg/L) for Nile tilapia [67] and the nitrite concentation remained below this limit throughout the four weeks. This is attributed to the conversion of nitrite to nitrate in ciculated aerobic water [62]. Ammonia and nitrite are toxic metabolites for the fish [72] and are not desired in fish farming systems. On the other hand, fish can tolerate high levels of nitrate much better than high levels of ammonia and nitrite [71]. However, both ammonia and nitrate concentrations need to be reduced for aquaponic systems. It is gratifying that ammonia and nitrate are desired for the growth of plants [73] and so their concentrations can be reduced by the hydroponics system. Therefore, the concentrations of these ions are relatively low in the water of both fishponds [Figs. 7B(a) and (b) and 7D(a) and (b)]. However, concentrations of inorganic nitrogen [Figs. 7B-D(a) and (b)] and phosphate [Figs. 7E(a) and (b)] are relatively high in the first week for both fishponds. This is attributed to low uptake of these materials by small plants [73]. Furthermore, both ammonia and nitrate concentrations of water in fishpond 2 are lower than in fishpond 1, which was due to the added PABC filter between the aquaculture and the hydroponic system. This has shown that these ions were also adsorbed by the PABC filter. The values of the last two parameters, DO [Figs. 7F(a) and (b)] and turbidity [Figs. 7G(a) and (b)], in both fishponds also increased from first the week to the fourth week. The DO concentration measures oxygen content in the water used by the fish for respiration and by autotrophic nitrifying bacteria for oxidation of ammonia to nitrite and nitrate [66]. This parameter can provide information about bacterial activity, photosynthesis, availability of nutrients, and stratification [71]. The increasing values of DO in the water of both fishponds was attributed to water circulation and the increasing quantity and length of the roots of the plants as the experiment

progressed. This increases the distribution of oxygen dissolved in water. Furthermore, it was observed that the DO values in the water of fishpond 2 [Fig. 7F(b)] are higher than in the water of fishpond 1 [Fig. 7F(a)] for all four weeks. These results were attributed to the PABC with spaces or pores, which acts as a filter in the water recirculation system. This can increase the diffusion of oxygen and increase the DO content in water [68]. Furthermore, the differences in DO between the two systems can also be attributed to higher ammonia content of water in fishpond 1, which could result in decreased DO in the water due to the presence of more autotrophic nitrifying bacteria for the nitrification process [74]. Likewise, turbidity [Figs. 7G(a) and (b)], which results from fish metabolism (feces, urine, and dissolved fish food), can cause increased stress on the fish and interfere with the penetration of light into the water. The low penetration of sun light, which was shielded by turbidity, can disrupt photosynthesis in aquatic plants, resulting in decreased oxygen levels in the water, wich can lead to fish death, harm to aquatic ecosystems, and decrease in water quality [65]. Turbitity could also be retained by the PABC filter and plant roots.

3.2.2. Efficiency of PABC for water treatment

The pH value has an important role in determining the anion and cation type and concentration in solution [70]. Therefore, the adsorption efficiency for inorganic nitrogen and phosphate ions by an adsorbent is dependent on pH values of water. On the other hand, the removal efficiency of turbidity and increasing efficiency of DO are dependent on the porous characteristics of the adsorbent. Efficiency percentages [Eq.(1)] in this study were calculated by comparison of values of water quality parameters in fishpond 1 and fishpond 2. The differences in these values are the result of the presence of the PABC filter. In this study, the percentage of removal efficiency for nitrite (Fig. 8b) and nitrate (Fig. 8c) decreased from the first to the third week and then increased in the fourth week. This is attributed to the pH values of water in fishpond 2, which are relatively alkaline [Fig. 7A(b)]. These conditions have resulted in a negative charge on the surface of the PABC in alkaline water, which repulsed the negatively charged nitrite and nitrate ions. In the case of ammonia the dominant species is the positively charged ammonium ion (NH_4^+ ions) at pH values below 9.26 (the ion dissociation constant (pKa) of NH_4^+/NH_3 buffer system = 9.26) [69]. Therefore, the positively charged ammonium ions were electrostatically attracted to the negatively charged surface of the PABC in slightly alkaline water. However, negatively charged phosphate ions were well chemisorbed via chelate complex formation on the surface of the PABC in slightly alkaline water [70]. This resulted in the phosphate removal efficiency being like that of the ammonium ions (Figs. 8a and d). It was observed that the removal efficiency of turbidity (Fig. 8e) and efficiency of increasing DO (Fig. 8f) grew during the first and the second week and then decreased after the third week. This is attributed to the high volume of pores within the PABC during the early stages of the culture, which can filter small particulate matter and aid oxygen diffusion to the water. These efficiencies of the PABC decreased after the third week. This is bcause the pores of the PABC became filled with small particulate wastes resulting in decreasing pore vacancy within the PABC. Furthermore, all of the efficiency percentages of the monitored parameters decreased the after third week. This was attributed to the lowering of the specific surface area and pore volume within the PABC by high content of adsorbed materials during the extended period of the fish culture. This includes the charge of the surface of the PABC being transformed to neutral, which does not provide electrostatic attraction. This demonstrated that the activated filter has begun to reach sorption saturation in the third week. Therefore, the PABC filter should be replaced with a new one after the fourth week of use.

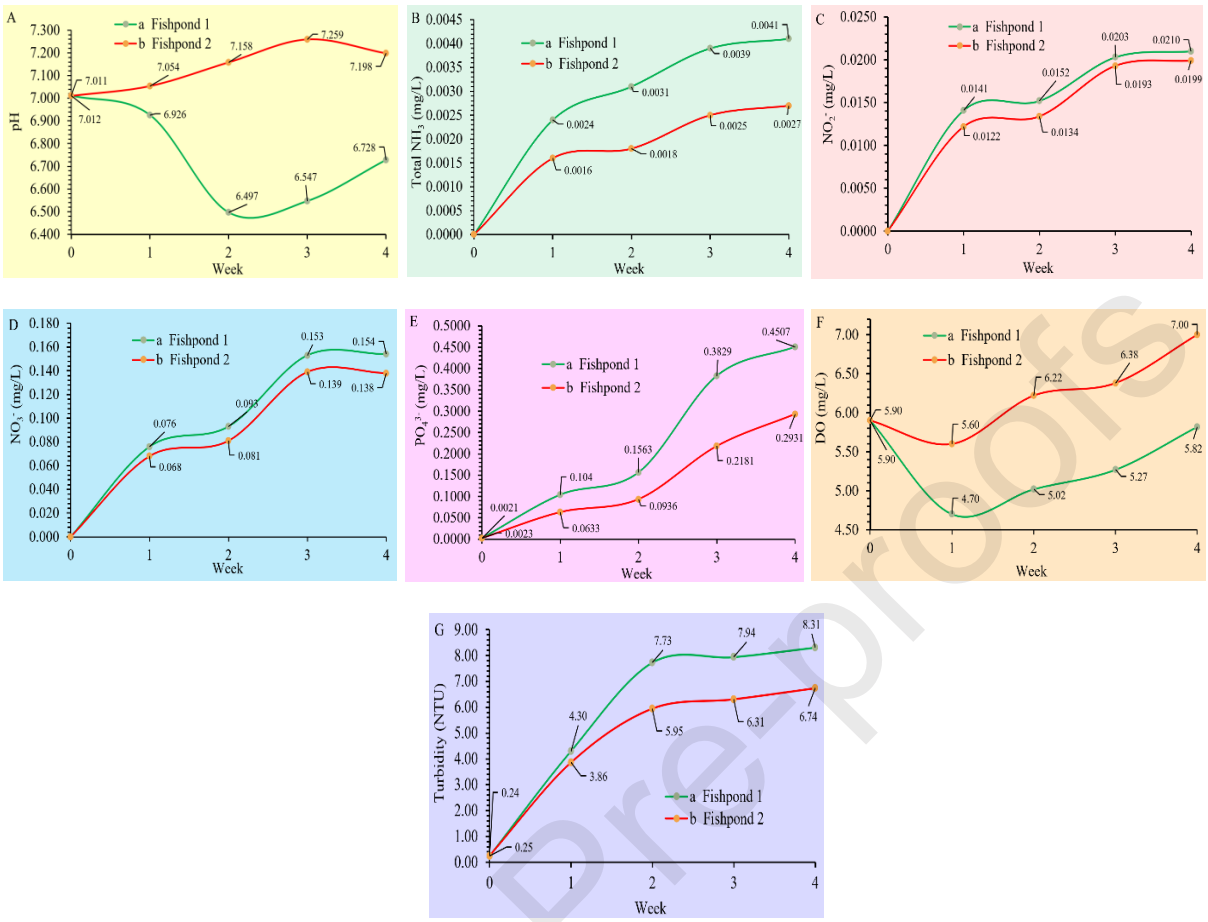

Fig. 7. Water analysis results of (A) pH, (B) total NH_3 concentration, (C) NO_2^- concentration, (D) NO_3^- concentration, (E) PO_4^{3-} concentration, (F) DO concentration, and (G) turbidity, of water in (a) fishpond 1, and (b) fishpond 2.

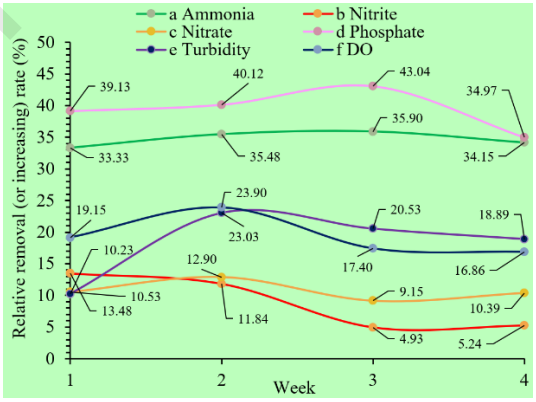

Fig. 8. Removal efficiency percentage of ammonia (a), nitrite (b), nitrate (c), phosphate (d), and turbidity (e), and increasing efficiency percentage of DO (f).

3.2.3. Growth rate of fish

In this study, the fish survival rate was 100% for both ASs experiments. These results showed that the quality of water in both ASs was good for fish survival. Growth rates of fish in all experiments were measured at the first day of the culture and weekly for the four weeks of the study. The results of measurements showed that the growth rates of fish in fishpond 2 (Fig. 9b) were relatively higher than growth rates of fish in fishpond 1 (Fig. 9a) for all weeks. This was attributed to the relatively high concentration of ammonia, nitrite, and nitrate, and acidic pH of water in fishpond 1 [Figs. 7A-D(a)], which can lower the blood oxygen-carrying capacity of fish and cause declines in growth and locomotor capacity [75]. High nitrate concentration and acidic pH of water causes methemoglobin formation, which is unable to reversibly bind oxygen and causes an inherent loss of oxygen transport capacity for fish [75]. It should be noted that ammonia concentrations in water in both fishponds [Figs. 7B(a) and (b)] were lower than the limit of 0.1 mg/L. Ammonium concentration higher than 0.1 mg/L can significantly inhibit growth in tilapia fingerlings [72]. In addition, pH values of water were maintained relatively close to the neutral pH level, which is suitable for fish growth [65]. These results correspond well with the study of Osman and El-Khateeb, 2016 [76] who used sand and activated carbon as filters for water treatment in AS.

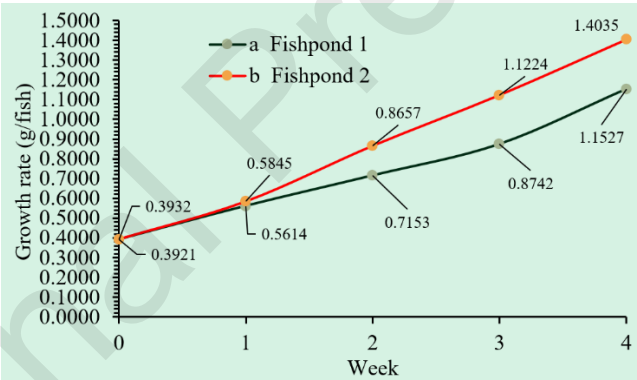

Fig. 9. Fish growth rates in (a) fishpond 1 (b) fishpond 2.

3.3.4. Growth rate of red oak lettuce

The plant harvesting was carried out after 4 weeks of cultivation because red oak is suitable for eating after about five weeks of cultivation (1 week seedling period and 4 weeks hydroponics culture) [77]. The results of plant growth measurements showed that all growth rate parameters of red oak lettuce grown in AS2 [Figs. 10A-D (b) and Table 4] were higher than those for the plants in AS1 [Figs. 10A-D (a) and Table 4] throughout the four weeks. This is attributed to higher inorganic nitrogen concentration and acidic water of aquaponics system 1 (AS1). Ammonia is toxic to plant cells by disrupting the thylakoid transmembrane proton gradient [75]. However, plants need nitrogen in form of nitrate and ammonium ion for growth and productivity [77].

Therefore, the growth rates of plants in AS2 are higher than those of plants in AS1. The relatively lower concentrations of inorganic nitrogen and phosphate materials in AS2 are due to the higher consumption of these species than in AS1 (Figs. 7B-E). Likewise, root length and root weight parameters of red oak lettuce exhibit a similar trend (Fig. 10B and Table 4), which is the result of ammonium and nitrate that stimulated lateral roots branching, and lateral roots elongation, respectively [78]. However, the growth of red oak lettuces in both ASs was poor during the first week. After that, the hair roots were developed, and the plants began to grow more rapidly. The slightly alkaline pH values of water in AS2 [Fig. 7A(b)] can result in more available phosphate than under more acidic conditions [67]. This effect resulted in a high soluble phosphate content in the ASs leading to increased phosphate uptake by the plants. Phosphorous has a significant role in increased root and shoot length and plant mass [79]. Therefore, all of growth parameters of red oak lettuce in AS2 are higher than in AS1. This involves the adsorption of ammonia by the PABC filter, which makes the water slightly alkaline. Furthermore, the PABC can also increase the DO in water of AS 2 [Fig. 7F(b)], which leads to more extensive conversion of nitrite to nitrate. All of the growth rate parameters of red oak lettuce in this study are similar to the results of a red oak lettuce hydroponics culture cultivated under sunlight in the study of Spalholz et al., 2020 [80].

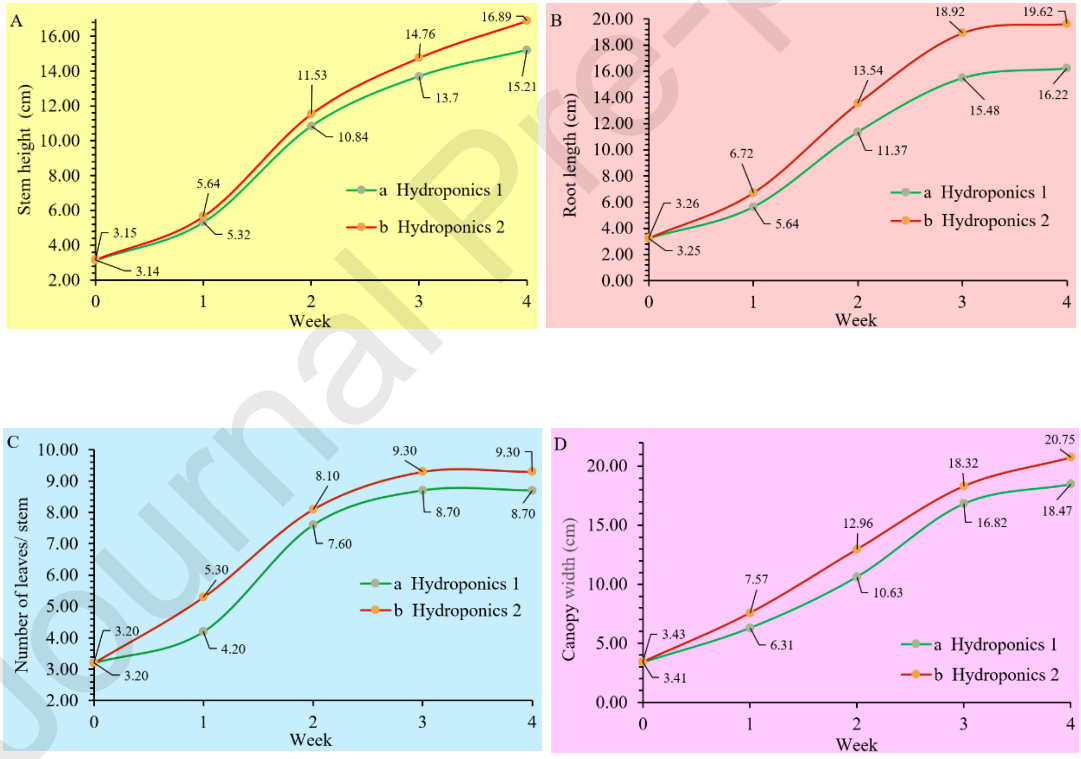

Fig. 10. Red oak lettuce growth parameters of (A) stem height, (B) root length, (C) number of leaves, and (D) canopy width in (a) hydroponics 1, and (b) hydroponics 2.

Table 4. Growth parameters after culture of red oak lettuce at fourth week.

Hydroponics No.	Fresh stem weight (g)	Dried stem weight (g)	Fresh root weight (g/stem)	Dried root weight (g/stem)	Dried leaves weight (g)	Fresh leaves weight (g)
1	16.36	1.36	4.75	1.26	0.15	1.34
2	17.92	1.47	5.01	1.69	0.17	1.43

4. Conclusion

The results of this research show that the one step production of PABC from PC by simple carbonization along with PAO in a closed system without the use of an inert gas or nitrogen in the temperature range of 400°C and 600°C could reduce the cost and production time. In this process, a small amount of oxygen from the air, which passes through the lid, acts as an activating agent for partial oxidation for PABC production. The PABC products exhibit good properties for water treatment with high potential utility in environmental applications. Diverse properties of the PABC products with highly disordered level of graphite, consist of new oxygenated functional groups (OH, C=O, C-O, and Si-O), retained oxide compounds (CaO, MgO, Na_2O, K_2O SiO_2), and relatively high specific surface area and micropore volume. These can act as electrostatic adsorbents, cation and anion exchange materials, and filters. These characteristics increase with increasing carbonization temperature from 400°C to 600°C. For materials produced at 600°C, the pore size of the PABC products fall in the range of micropores (< 2 nm) with a small content of mesopores and macropores. In addition, BET specific surface area of 270.27 m^2/g was observed, which has the potential for adsorption of pollutants for water treatment. Therefore, the PABC produced at 600°C was collected as filter for immobilization of pollutants from solution in AS. The presence of the PABC filter resulted in the reduction of total NH_3, NO_2^-, NO_3^-, PO_4^{3-}, and turbidity and increase in DO in water of the AS throughout all four weeks of the experiment with efficiency percentages of 33.33-35.90%, 4.93-13.43%, 9.15-12.90%, 34.97-43.04%, 10.23-23.90%, and 16.86-23.90%, respectively. The PABC filter could maintain water pH in a mildly alkaline range throughout the experiment. These conditions are suitable for the culture of tilapia and red oak lettuce. However, the efficiency of the PABC decreased after the third week of the culture, as it began to reach sorption saturation. Therefore, the PABC filter should be replaced with a new one after four weeks of use. The used PABC can be reactivated and reused to grow vegetables. However, this will require further research. In addition, the optimization of parameters such as air flow rate and amount of air needed for activation of PC will also require further research.

CRediT authorship contribution statement

Sumrit Mopoung: Formal analysis, Writing – original draft, Methodology, Validation, Writing – review & editing, Supervision, Project administration, Funding acquisition, Conceptualization,

Commented on previous versions of the manuscript, Read and approved the final manuscript. **Suthasinee Pantho:** Methodology, Investigation, Data curation, Validation, Commented on previous versions of the manuscript, Read and approved the final manuscript.

Declaration of Competing Interest

The authors declare that they have no known competing financial interests or personal relationships that could have appeared to influence the work reported in this paper.

Acknowledgements

The authors acknowledge Chemistry Department and Science Lab Center, Faculty of Science, Naresuan University, for all the analyses and Institutional Review Board of the Committee on Animal Execution for Science, Naresuan University for approved the animal study protocol (protocol code 61 01 007).

Availability of data and materials

The datasets used or analyzed during the current study are available from the corresponding author on reasonable requests.

References

[1] Z. Chen, Y. Guo, L. Luo, Z. Liu, W. Miao, Y. Xia, A critical review of hydrochar based photocatalysts by hydrothermal carbonization: synthesis, mechanisms, and applications, Biochar. 6 (2024) 74, https://doi.org/10.1007/s42773-024-00364-9.

[2] J.X. Liao, P.S. So, S. Bordoloi, D.N. Li, H.R.Yuan, Y. Chen, L.Q. Xin, Plant performance and soil–plant carbon relationship response to different biochar types, Biochar. 6 (2024) 75, https://doi.org/10.1007/s42773-024-00355-w.

[3] Z. Sun, L. Dai, P. Lai, F. Shen, F. Shen, W. Zhu, Air oxidation in surface engineering of biochar-based materials: a critical review, Carbon. Res. 1 (2022) 32, https://doi.org/10.1007/s44246-022-00031-3.

[4] V. Hadiya, K. Popat, S. Vyas, S. Varjani, M. Vithanage, V.K. Gupta, A.N. Delgado, Y. Zhou, P.L. Show, M. Bilal, Z. Zhang, M. Sillanpää, S.S. Mohanty, Z. Patel, Biochar production with amelioration of microwave-assisted pyrolysis: Current scenario, drawbacks and perspectives, Bioresour. Technol. 355 (2022) 127303, https://doi.org/10.1016/j.biortech.2022.127303.

[5] P.R. Yaashikaa, P.S. Kumar, S. Varjani, A.A. Saravanan, Critical review on the biochar production techniques, characterization, stability and applications for circular bioeconomy, Biotechnol. Rep. 28 (2020) e00570. https://doi.org/10.1016/j.btre.2020.e00570.

[6] H.K.S. Panahi, M. Dehhaghi, Y.S. Ok, A.S. Nizami, B. Khoshnevisan, S.I. Mussatto, M. Aghbashlo, M. Tabatabaei, S.S. Lam, A comprehensive review of engineered biochar:

Production, characteristics, and environmental applications, J. Cleaner. Prod. 270 (2020) 122462, https://doi.org/10.1016/j.jclepro.2020.122462.

[7] G.S. dos Reis, S. Petnikota, H.P. de Oliveira, I.A.S. de Brum, M. Thyrel, G.L. Dotto, E.C. Lima, M. Naushad, T. Hu, U. Lassi, A. Grimm, Statistics design for the synthesis optimization of lignin-sulfonate sulfur-doped mesoporous carbon materials: promising candidates as adsorbents and supercapacitors materials, Sci. Rep. 14 (2024) 23354, https://doi.org/10.1038/s41598-024-75003-1.

[8] A. Grimm, G.S. dos Reis, S.G. Khokarale, S. Ekman, E.C. Lima, S. Xiong, M. Hultberg, Shiitake spent mushroom substrate as a sustainable feedstock for developing highly efficient nitrogen-doped biochars for treatment of dye-contaminated water, J. Water Process Eng. 56 (2023) 23354, https://doi.org/10.1016/j.jwpe.2023.104435.

[9] A. Grimm, F. Chen, G.S. dos Reis, V.M. Dinh, S. G. Khokarale, M. Finell, J.P. Mikkola, M. Hultberg, G.L. Dotto, S. Xiong, Cellulose fiber rejects as raw material for integrated production of pleurotus spp. mushrooms and activated biochar for removal of emerging pollutants from aqueous media, ACS Omega. 6(6) (2023) 5361-5376, https://doi.org/10.1021/acsomega.2c06453.

[10] T. Britannica, Air, Encyclopedia Britannica, 2024. https://www.britannica.com/science/air. Accessed 23 September 2024.

[11] M. Ghorbani, P. Konvalina, R.W. Neugschwandtner, G. Soja, J. Bárta, W.H. Chen, E. Amirahmadi, How do different feedstocks and pyrolysis conditions effectively change biochar modification scenarios? A critical analysis of engineered biochars under H_2O_2 oxidation, Energy. Convers. Manage. 300 (2024) 117924, https://doi.org/10.1016/j.enconman.2023.117924.

[12] G. Ranalli, E. Zanardini, C. Sorlini, Biodeterioration – Including Cultural Heritage. in: M. Schaechter (ed), Encyclopedia of Microbiology, third ed., Academic Press, Massachusetts, 2009, pp. 191-205. https://doi.org/10.1016/B978-012373944-5.00132-2.

[13] N. Mburu, D.P. Rousseau, J.J. Van Bruggen, P.N. Lens, Use of the macrophyte Cyperus papyrus in wastewater treatment in: The Role of Natural and Constructed Wetlands in Nutrient Cycling and Retention on the Landscape. Springer, Cham, 2015, pp. 293-314.

[14] M.T.M.H. Hamad, Comparing the performance of *Cyperus papyrus* and *Typha domingensis* for the removal of heavy metals, roxithromycin, levofloxacin and pathogenic bacteria from wastewater, Environ. Sci. Eur. 35 (2023) 61, https://doi.org/10.1186/s12302-023-00748-x.

[15] W.O. Toamah, A.K. Fadhil, Removing crude oil from water by activated carbon prepared from dried papyrus plant, Egypt. J. Chem. 64(10) (2021) 5879 – 5884, https://doi.org/10.21608/ejchem.2021.79030.3868.

[16] S.A. Gorrazzi, D. Massazza, A. Pedetta, L. Silva, B. Prados, G. Fouga, S. Bonanni, Biochar as a substitute for graphite in microbial electrochemical technologies, RSC Sustain. 1 (2023) 1200-1210, https://doi.org/10.1039/D3SU00041A.

[17] S. Goddek, A. Joyce, Wuertz, O. Körner, I. Bläser, M. Reuter, K.J. Keesman, Decoupled aquaponics systems. in: S. Goddek, A. Joyce, B. Kotzen, G.M. Burnell (eds.), Aquaponics food production systems, Springer, Heidelberg, 2019, pp. 201-209. https://doi.org/10.1007/978-3-030-15943-6_8.

[18] W. Lennard, S. Goddek, Aquaponics Food Production Systems. Springer, Cham, 2019. https://doi.org/10.1007/978-3-030-15943-6_5. Accessed 23 September 2024.

[19] M. Krastanova, I. Sirakov, S. Ivanova-Kirilova, D. Yarkov, P. Orozova, Aquaponic systems: biological and technological parameters, Biotechnol. Biotechnol. Equip. 36(1) (2022) 305–316, https://doi.org/10.1080/13102818.2022.2074892.

[20] A. Espinosa-Moya, A. Álvarez-González, P. Albertos-Alpuche, R. Guzmán-Mendoza, R. Martínez-Yáñez, Growth and development of herbaceous plants in aquaponic systems, Acta. Universitaria. 28(2) (2018) 1-8. https://doi.org/10.15174/au.2018.1387.

[21] Z. Hu, J.W. Lee, K. Chandran, S. Kim, A.C. Brotto, S.K. Khanal, Effect of plant species on nitrogen recovery in aquaponics, Bioresour. Technol. 188 (2015) 92-98, https://doi.org/10.1016/j.biortech.2015.01.013.

[22] ASTM, Standard Test Methods for Moisture in Activated Carbon ASTM D2867-17. American Society for Testing and Materials, Pennsylvania, 2023.

[23] ASTM, Standard Test Method for Total Ash content of Activate Carbon: ASTM D 2866-11. American Society for Testing and Materials, Pennsylvania, 2011

[24] ASTM, Standard Test Method for Volatile Matter Content of Activate Carbon ASTM D 5832-98. American Society for Testing and Materials, Pennsylvania, 1998.

[25] ASTM, Standard Practice for Proximate Analysis of Coal and Coke: ASTM D3172-13(2021)e1. American Society for Testing and Materials, Pennsylvania, 2021.

[26] T.E. Waters, M.T. Alexander, D.G. Wahman, Temperature impact on monochloramine, free ammonia, and free chlorine indophenol methods, Water. Pract. Technol. 16(1) (2021) 135-145, https://doi.org/10.2166/wpt.2020.104.

[27] N.V. Sreekumar, B. Narayana, P. Hegde, B.R. Manjunatha, B.K. Sarojini, Determination of nitrite by simple diazotization method, Microchem. J. 74(1) (2003) 27-32, https://doi.org/10.1016/S0026-265X(02)00093-0.

[28] M.A. Jaworski, G.L. Siri, M.L. Casella, A simple and sensitive spectrophotometric determination of nitrate and nitrite in water samples. Asian. J. Research. Chem. 4(11) (2011) 1655-1660.

[29] K. Motter, L. Hartley, Standard operating procedure for the analysis of fresh water samples for orthophosphorus CCAL 34D.1. Cooperative Chemical Analytical Laboratory, College of Forestry, Oregon State University, Oregon, 2019, pp. 1-12.

[30] J.H. Carpenter, The Chesapeake bay institute technique for the Winkler dissolved oxygen method, Limnol. Oceanogr. 10 (1965) 141-143.

[31] K.K.B.S. Babu, M. Nataraj, M. Tayappa, Y. Vyas, R.K. Mishra, B. Acharya, Production of biochar from waste biomass using slow pyrolysis: studies of the effect of pyrolysis temperature and holding time on biochar yield and properties, Mater. Sci. Energy Technol. 7 (2024) 318-334, https://doi.org/10.1016/j.mset.2024.05.002.

[32] E.A. Varol, Ü. Mutlu, TGA-FTIR Analysis of biomass samples based on the thermal decomposition behavior of hemicellulose, cellulose, and lignin, Energies. 16(9) (2023) 20233674, https://doi.org/10.3390/en16093674.

[33] Z. Zha, K. Wu, Z. Ge, Y. Ma, M. Zeng, Y. Wu, Y. Tao, H. Zhang, Effect of oxygen on thermal behaviors and kinetic characteristics of biomass during slow and flash pyrolysis processes, Combust. Flame. 247 (2023) 112481, https://doi.org/10.1016/j.combustflame.2022.112481.

[34] O. Tursunov, K. Zubek, J. Dobrowolski, G. Czerski, P. Grzywacz, Effect of Ni/Al_2O_3-SiO_2 and Ni/Al_2O_3-SiO_2 with K_2O promoter catalysts on H_2, CO and CH_4 concentration by CO_2 gasification of *Rosa Multiflora* biomass, Oil. Gas. Sci. Technol. 72(6) (2017) 37. https://doi.org/10.2516/ogst/2017037.

[35] O. Oginni, K. Singh, J.W. Zondlo, Pyrolysis of dedicated bioenergy crops grown on reclaimed mine land in West Virginia, J. Anal. Appl. Pyrolysis. 123 (2017) 319-329, https://doi.org/10.1016/j.jaap.2016.11.013.

[36] M.A. Naeem, M. Khalid, M. Arshad, R. Ahmad, Yield and nutrient composition of biochar produced from different feedstocks at varying pyrolytic temperatures, Pak. J. Agri. Sci. 51(1) (2014) 75-82.

[37] N.S. Jacobson, M.A. Kuczmarski, B.A. Kowalski, Vaporization of protective oxide films into different gas atmospheres. Oxid. Met. 93 (2020) 247–282, https://doi.org/10.1007/s11085-019-09921-1.

[38] K.S.P. Karunadasa, C.H. Manoratne, H.M.T.G.A. Pitawala, R.M.G. Rajapakse, Thermal decomposition of calcium carbonate (calcite polymorph) as examined by in-situ high-temperature X-ray powder diffraction, J. Phys. Chem. Solids. 134 (2019) 21-28, https://doi.org/10.1016/j.jpcs.2019.05.023.

[39] K. Joseph, T. Gnanasekaran, Thermoanalytical study of the reaction of potassium carbonate with ferric oxide, Thermochimica Acta. 342 (1999) 153-160, https://doi.org/10.1016/S0040-6031(99)00337-8.

[40] I. Pioro, R. Duffey, 4-Current and future nuclear power reactors and plants. in: T.M. Letcher (ed), Managing Global Warming. Academic Press, Massachusetts, 2019, pp. 117-197,

https://doi.org/10.1016/B978-0-12-814104-5.00004-1.

[41] A.L. Smith, C. Guéneau, J.L. Flèche, S. Chatain, O. Beneš, R.J.M. Konings, Thermodynamic assessment of the Na-O and Na-U-O systems: margin to the safe operation of SFRs, J. Chem. Thermodyn. 114 (2017) 93-115, https://doi.org/10.1016/j.jct.2017.04.003.

[42] A. Altıkat, M.H. Alma, A. Altıkat, M.E. Bilgili, S. Altıkat, A comprehensive study of biochar yield and quality concerning pyrolysis conditions: a multifaceted approach, Sustainability. 16(2) (2024) 937, https://doi.org/10. 3390/su16020937.

[43] A.A. El hadad, D. Carbonell, V. Barranco, A. Jiménez-Morales, B. Casal, J.C. Galván, Preparation of sol-gel hybrid materials from 3-methacryloxypropyltrimethoxysilane and tetramethylorthosilicate: study of the hydrolysis and condensation reactions, Colloid. Polym. Sci. 289(17-18) (2011) 1875-1883, https://doi.org/10.1007/s00396-011-2504-y.

[44] N. Rangelova, L. Radev, S. Nenkova, I.M.M. Salvado, M.H.V. Fernandes, M. Herzog, Methylcellulose/SiO_2 hybrids: sol-gel preparation and characterization by XRD, FTIR and AFM, Cent. Eur. J. Chem. 9(1) (2011) 112-118, https://doi.org/10.2478/s11532-010-0123-y.

[45] J.D. Rodriguez-Blanco, S. Shaw, L.G. Benning. The kinetics and mechanisms of amorphous calcium carbonate (ACC) crystallization to calcite, via vaterite, Nanoscale. 3(1) (2011) 265-271. https://doi.org/10.1039/c0nr00589d. Epub 2010 Nov 10. PMID: 21069231.

[46] X. Bertran, G. Chollon, J. Dentzer, R. Gadiou, S. Fouquet, M.A. Dourges, F. Rebillat, Oxidation behavior at moderate temperature under dry and wet air of phenolic resin-derived carbon, Thermochim. Acta. 649 (2017) 13-21, https://doi.org/10.1016/j.tca.2016.12.013.

[47] S. Yadav, S.K. Padhi, Ch. Srinivasulu, K.L. Naidu, Raman spectroscopy study on the vibration and structural changes of graphene oxide: effect of laser power and time, J. Ovonic. Res. 20(2) (2024) 221-232, https://doi.org/10.15251/JOR.2024.202.221.

[48] Y. Liu, X. Liu, W. Dong, L. Zhang, Q. Kong, W. Wang, Efficient adsorption of sulfamethazine onto modified activated carbon: A plausible adsorption mechanism, Sci. Rep. 7 (2017) 12437, https://doi.org/10.1038/s41598-017-12805-6.

[49] P. Puech, M. Kandara, G. Paredes, L. Moulin, E. Weiss-Hortala, A. Kundu, N. Ratel-Ramond, J.M. Plewa, R. Pellenq, M. Monthioux, Analyzing the Raman spectra of graphenic carbon materials from kerogens to nanotubes: what type of information can be extracted from defect bands?, J. Carbon. Res. 5(4) (2019) 1-19, https://doi.org/10.3390/c5040069.

[50] K.A. Janulewicz, T. Fok, B. Bartosewicz, A. Bartnik, H. Fiedorowicz, P. Wachulak, Structural stability and disorder level of moderately reduced paper-like graphene oxide investigated with Micro-Raman analysis, Materials. 17(4) (2024) 877, https://doi.org/10.3390/ma17040877.

[51] S. Darmawan, N.J. Wistara, G. Pari, A. Maddu, W. Syafii, Characterization of lignocellulosic biomass as raw material for the production of porous carbon-based

materials, BioRes. 11(2) (2016) 3561-3574, https://doi.org/10.15376/biores.11.2.3561-3574.

[52] I. Vydrina, A. Malkov, K. Vashukova, I. Tyshkunova, L. Mayer, A. Faleva, S. Shestakov, E. Novozhilov, D. Chukhchin, A new method for determination of lignocellulose crystallinity from XRD data using NMR calibration, Carbohydr. Polym. Technol. Appl. 5 (2023) 100305, https://doi.org/10.1016/j.carpta.2023.100305.

[53] S.M. Lee, S.H. Lee, J.S. Roh, Analysis of activation process of carbon black based on structural parameters obtained by XRD analysis, Crystals. 11 (2012) 153, https://doi.org/10.3390/cryst11020153.

[54] S. Basfar, S. Elkatatny, Micronized calcium carbonate to enhance water-based drilling fluid properties, Sci. Rep. 13 (2023) 18295, https://doi.org/10.1038/s41598-023-45776-y

[55] G. Dercz, K. Prusik, L. Pajak, R. Pielaszek, J.J. Malinowski, W. Pudlo, Structure studies on nanocrystalline powder of MgO xerogel prepared by the sol-gel method, Mater. Sci.-Pol. 27(1) (2009) 201-207.

[56] R. Kumar, H. Miyaoka, K. Shinzato, T. Ichikawa, Analysis of sodium generation by sodium oxide decomposition on corrosion resistance materials: a new approach towards sodium redox water- splitting cycle, RSC Adv. 11 (2021) 21017, https:// doi.org/ 10.1039/d1ra02671b.

[57] C. Pakpahan, S. Arita, T.I. Sari, L.N. Komariah, F. Hadiah, N. Renaldi, Extraction of K_2CO_3 from empty palm fruit bunch ash and properties analysis, Jurnal Teknik Kimia. 30(1) (2024) 67-79, https://doi.org/10.36706/jtk.v30i1.2355.

[58] Y.H. Chen, K.L. Lin, C.C. Lin, Interfacial reactions between Si and SiO_2 with ceramic additives, Ceramics. 5 (2022) 44-54, https://doi.org/10.3390/ceramics5010005.

[59] N. Khan, D. Dollimorey, K. Alexander, F.W. Wilburn. The origin of the exothermic peak in the thermal decomposition of basic magnesium carbonate. Thermochimica Acta. 367-368 (2001) 321-333, https://doi.org/10.1016/S0040-6031(00)00669-9.

[60] R.V. Siriwardane, J.A. Poston Jr., C. Robinson, T. Simonyi, Effect of additives on decomposition of sodium carbonate: Precombustion CO_2 capture sorbent regeneration, Energy Fuels. 25(3) (2011) 1284-1293, https://doi.org/10.1021/ef101486m.

[61] W. Chai, F. Wang, Z. Miao, N. Che, Hydrophilic porous activated biochar with high specific surface area for efficient capacitive deionization, Desalin. Water. Treat. 320 (2024) 100617, https://doi.org/10.1016/j.dwt.2024.100617.

[62] Y.H. Wu, Q.F. Chen, J.N. Wang, T. Liu, W.Y. Zhao, Substrates, plants, and their combinations for water purification of urban household aquaponics systems, Int. J. Environ. Res. Public. Health. 19 (2022) 10276, https://doi.org/10.3390/ijerph191610276.

[63] H. Rezaei, S. Rastegar, S. Naseri, Application of chitosan and activated carbon nano-composite in removal of nitrite, phosphate, and ammonia from aquaculture wastewater, Avicenna. J. Environ. Health. Eng. 6(2) (2019) 106-112, https://doi.org/10.34172/ajehe.2019.14.

[64] M. Gholipour, P. Mehrabanjoubani, A. Abdolzadeh, M. Raghimi, S. Seyedkhademi, E. Karimi, H.R. Sadeghipour, Facilitated decrease of anions and cations in influent and effluent of sewage treatment plant by vetiver grass (*Chrysopogon zizanioides*): the uptake of nitrate, nitrite, ammonium, and phosphate, Environ. Sci. Pollut. Res. Int. 27(17) (2020) 21506-21516, https://doi.org/10.1007/s11356-020-08677-5.

[65] C.L. Kok, I.M.B.P. Kusuma, Y.Y. Koh, H. Tang, A.B. Lim, Smart aquaponics: an automated water quality management system for sustainable urban agriculture, Electronics. 13 (2024) 820, https:// doi.org/10.3390/electronics13050820.

[66] A. Princic, I.I. Mahne, F. Megusar, E.A. Paul, J.M. Tiedje, Effects of pH and oxygen and ammonium concentrations on the community structure of nitrifying bacteria from wastewater, Appl. Environ. Microbiol. 64(10) (1998) 3584-3590, https:// doi.org/10.1128/AEM.64.10.3584-3590.1998.

[67] V.P. Lobanov, D. Combot, P. Pelissier, L. Labbé, A. Joyce, Improving plant health through nutrient remineralization in aquaponic systems, Front. Plant. Sci. 12 (2021) 683690, https:// doi.org/10.3389/fpls.2021.683690.

[68] F. Nadilla, N. Wahyuni, S. Maulizar, Fitriani, Y. Amri, Medium and filter from activated carbon in aquaponics system (*Oryza sativa* and *Oreochromis niloticus*) to improve water quality, IOP Conf. Series: Mater. Sci. Eng. 725 (2020) 012068, https:// doi.org/10.1088/1757-899X/725/1/012068.

[69] G. Salbitani, S. Carfagna, Ammonium utilization in microalgae: a sustainable me,hod for wastewater treatment, Sustainability. 13 (2021) 956, https://doi.org/10.3390/su13020956.

[70] M. Sayadi, M. Farasati., M.G. Mahmoodlu, P.R. Charati, Removal of nitrate, ammonium, and phosphate from water using conocarpus and paulownia plant biochar, Iran. J. Chem. Chem. Eng. 39(4) (2020) 205-222, https://doi.org/10.30492/ijcce.2019.35183.

[71] T. Manikandarajan, K. Ramamoorthy, S. Shanmugasundaram, A. Eswar, K. Kathirvel, G. Sankar, Determination of ammonia, nitrate and nitrite concentrations in marine water samples with cultured marine ornamental fish water sample analysis, Int. Lett. Nat. Sci. 42 (2015) 69-75, https://doi.org/10.18052/www.scipress.com/ILNS.42.69.

[72] L. Silva, E. Gasca-Leyva, E. Escalante, K.M. Fitzsimmons, D.V. Lozano, Evaluation of biomass yield and water treatment in two aquaponic systems using the dynamic root floating technique (DRF), Sustainability. 7(11) (2015) 15384-15399, https://doi.org/10.3390/su71115384.

[73] J. Schullehner, L. Stayner, B. Hansen, Nitrate, nitrite, and ammonium variability in drinking water distribution systems, Int. J. Environ. Res. Public. Health. 14(3) (2017) 276, https://doi.org/10.3390/ijerph14030276.

[74] S.M. Ahari, R.J. Yangejeh, A.H. Mahvi, Y.D. Shahamat, A.A. Takdastan, New method for the removal of ammonium from drinking water using hybrid method of modified zeolites /

catalytic ozonation, Desalin. Water. Treat. 170 (2019) 148-157, https://doi.org/10.5004/dwt.2019.24619.

[75] D.F. Gomez Isaza, R.L. Cramp, C.E. Franklin, Simultaneous exposure to nitrate and low pH reduces the blood oxygen-carrying capacity and functional performance of a freshwater fish, Conserv. Physiol. 8(1) (2020) coz092, https://doi.org/10.1093/conphys/coz092.

[76] G.A. Osman, M.A. El-Khateeb, Impact of water contamination on tilapia (*Oreochromis niloticus*) fish yield, Int. J. ChemTech. Res. 9(12) (2016) 166-181.

[77] D. Stefanelli, S. Winkler, R. Jones, Reduced nitrogen availability during growth improves quality in red oak lettuce leaves by minimizing nitrate content, and increasing antioxidant capacity and leaf mineral content, Agric. Sci. 2 (2011) 477-486, https://doi.org/10.4236/as.2011.24061.

[78] T. Hachiya, H. Sakakibara, Interactions between nitrate and ammonium in their uptake, allocation, assimilation, and signaling in plants, J. Exp. Bot. 68(10) (2017) 2501-2512, https://doi.org/10.1093/jxb/erw449.

[79] P. Prasad, S. Kalam, N.K. Sharma, A.R. Podile, S.N. Das, Phosphate solubilization and plant growth promotion by two Pantoea strains isolated from the flowers of *Hedychium coronarium L.*, Front. Agron. 4 (2022) 990869, https://doi.org/10.3389/fagro.2022.990869.

[80] H. Spalholz, P. Perkins-Veazie, R. Hernández, Impact of sun-simulated white light and varied blue:red spectrums on the growth, morphology, development, and phytochemical content of green- and red-leaf lettuce at different growth stages, Sci. Hortic. 264 (2020) 109195, https://doi.org/10.1016/j.scienta.2020.109195.

Declaration of Competing Interest

The authors declare that they have no known competing financial interests or personal relationships that could have appeared to influence the work reported in this paper.

Graphical Abstract

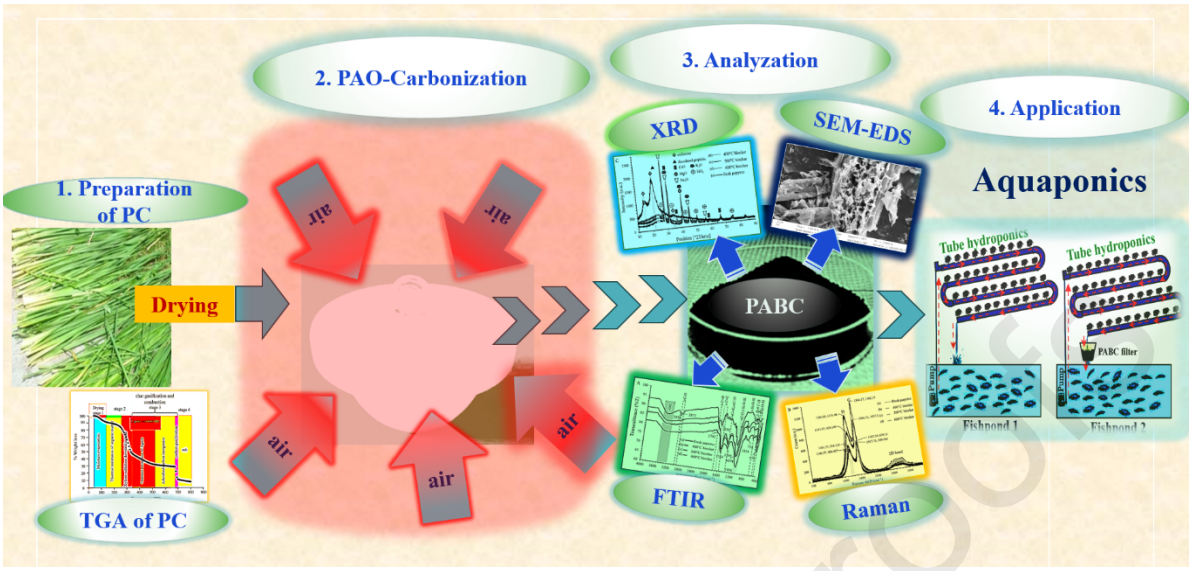

Highlights

• Papyrus culm derived activated biochar production by single step air activation could reduce the cost and production time.

• The best properties of the activated biochar were achieved with activation at 600°C.

• Derived activated biochar could maintain water for culture of tilapia and red oak lettuce.